International Journal of Plasticity 72 (2015) 185–199

Contents lists available at ScienceDirect

International Journal of Plasticity

journal homepage: www.elsevier.com/locate/ijplas

Pseudoelasticity in Fe_3Ga with boron-A combined atomistic–micromechanical treatment

A. Ojha, L. Patriarca, H. Sehitoglu*

Department of Mechanical Science and Engineering, University of Illinois at Urbana-Champaign, 1206 W. Green St., Urbana, IL 61801, USA

ARTICLE INFO

Article history:
Received 11 March 2015
Received in revised form 30 April 2015
Available online 11 June 2015

Keywords:
Pseudoelasticity
Fe_3Ga-B
DFT
DIC
Pseudotwinning

ABSTRACT

The Fe_3Ga base alloy is known to exhibit pseudoelasticity and the solute hardened Fe_3GaB holds considerable promise as well. The present work aims at developing a theoretical model to establish the critical twinning stress in Fe_3Ga with varying boron concentration. The theoretical model is based on the atomistic–micromechanical approach where we utilize density functional theory and Peierls Nabarro formalism at an atomic scale and the Eshelbian anisotropic elasticity at microscale. Using local strain measurements at the grain scale, we also show the experimental evidence of effect of boron in elevating the twinning stress in Fe_3Ga. The work calculates the interaction energies associated with the presence of boron in octahedral, tetrahedral and xenohedral sites in the $D0_3$ lattice and the transition from octahedral to xenohedral sites upon twinning. The model distinguishes the elevation of twinning stress depending on the interstitial site and the transition between the sites.

1. Introduction

The study of metals that exhibits reversibility of deformation has been of interest for many years (Otsuka and Wayman, 1998; Tanaka et al., 1986; Thamburaja and Anand, 2002; Wang et al., 2008). Most works focus on shape memory alloys which undergo reversible phase transformation, and considerable effort has been made to model their mechanical behavior (Gall et al., 2001; Hartl et al., 2010; Moumni et al., 2008). There is another emerging class of alloys that exhibits reversibility via twinning/detwinning and reversible slip mechanisms. The potential advantage of these alloys is that by alloying, the yield stress can be altered without affecting the temperature interval for reversibility. The iron–gallium and iron–aluminum alloys fall into this category. The Fe_3Ga alloy exhibits pseudoelasticity where strains as large as 5% can be recovered upon unloading (Yasuda et al., 2013; Yasuda and Umakoshi, 2011). The advantage of an alloy such as Fe_3Ga is the potentially large pseudoelastic temperature interval compared to shape memory alloys. Pseudoelasticity is a consequence of reversible pseudotwinning, a form of twinning in ordered alloys, and reversible slip. Alloying of Fe–Ga crystals with boron has proven beneficial for improving the ductility and flow stress (Gao et al., 2009). In this paper, we explore the elevation in critical twinning stress in the $D0_3$ ordered Fe_3Ga crystals with boron with atomistic–micromechanical treatments. We specifically investigate pseudotwinning, motivated by the early research on the Fe_3Ga system including modeling and experimental efforts. We use high resolution Digital Image Correlation (DIC) technique to precisely pinpoint the onset of twinning in Fe_3Ga and Fe_3GaB crystals. We conduct Density Functional Theory (DFT) calculations, utilize micromechanics with anisotropic

* Corresponding author.
E-mail address: huseyin@illinois.edu (H. Sehitoglu).

http://dx.doi.org/10.1016/j.ijplas.2015.05.013
0749-6419/

elasticity, fault energy curves, determine interaction energies for varying solute concentrations which are in turn combined for macroscopic critical twinning stress determination. We then extend the present analysis on Fe_3Ga for various boron concentrations emphasizing the promise of such alloys and need for further experimental work.

Generally, pseudoelasticity in shape memory alloys is based on the thermoelastic transformation where stress-induced martensite transforms back and forth upon loading and unloading (Otsuka and Wayman, 1998). However, recent studies (Umakoshi et al., 2005; Yasuda et al., 2007a,b,c; Yasuda and Umakoshi, 2011) show that Fe_3Al and Fe_3Ga exhibit pseudoelasticity via reversible slip and pseudotwinning, without martensite transformation. Pseudotwins are different from the conventional reflective twins because different species of atoms occupy the mirror position. The occurrence of pseudotwinning in Fe_3Al and Fe_3Ga provides advantages compared to martensite transformation as there is zero volume change and the resultant crystal is not internally twinned. In fact, the lack of multitude of interfaces reduces dissipation. Therefore, these factors should assist the reversibility of deformation by reducing the plasticity and minimizing the hysteresis respectively.

As seen in the phase diagram (Ikeda et al., 2002), the Fe_3Ga occur in various crystallographic structures such as α (bcc), $L1_2$, $D0_3$ or combination of phases for different compositions of gallium and annealing temperature. Of these phases, we are interested in the Fe_3Ga (25 at.%Ga) samples consisting of single $D0_3$ phase which exhibit perfect pseudoelasticty with a recovery ratio of one when deformed at low temperature (93 K) (Yasuda et al., 2005; Yasuda and Umakoshi, 2011). The recovery ratio (r) is a measure of pseudoelasticity of a material. In other words, it quantifies how much of the inelastic strain accumulated during loading is recovered upon unloading. It is defined as the ratio of the difference of the maximum plastic strain ($\varepsilon_p^{\max}$) and the residual strain (ε_r) to that of the maximum plastic strain, and can be written as follows:

$$r = \frac{\varepsilon_p^{\max} - \varepsilon_r}{\varepsilon_p^{\max}} \tag{1}$$

In Fig. 1, we illustrate the pseudoelastic response of [012] oriented Fe_3Ga crystal deformed in tension at room temperature. The recovery ratio is experimentally determined to be 0.83 with the values for $\varepsilon_p^{\max}$ and the residual strain ε_r as 2.9% and 0.5% respectively. It is important to note that the recovery ratio depends on several factors such as composition of alloying elements, test temperature, crystal orientation, degree of order and heat treatment (Yasuda and Umakoshi, 2011). For the case of Fe_3Ga (25 at.%Ga), the recovery ratio is found to decrease with an increase in temperature (above 93 K) or an increase in gallium concentration beyond 25 at.%. Additionally, with an increase in the $L1_2$ phase, the recovery ratio is found to decrease (Yasuda et al., 2005). This is because pseudotwins are unlikely to occur in the $L1_2$ phase due to significantly high energy barrier and high twinning stress (492 MPa) (Wang and Sehitoglu, 2014b), as validated by recent simulation results. Tension-compression asymmetry is observed in the $D0_3$ Fe_3Ga, and therefore, a pseudotwin formed in compression cannot form in

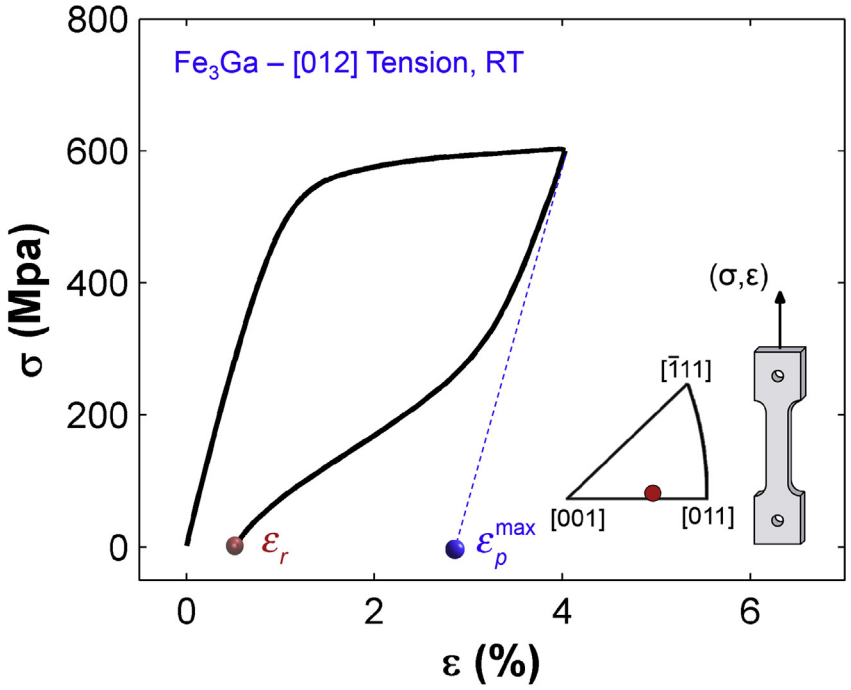

Fig. 1. The pseudoelastic stress-strain response of [012] oriented Fe_3Ga single crystal subjected to tension at room temperature (RT).

tension and vice versa. Experiments show that pseudotwinning follows Schmid law to a first approximation, and twinning pseudoelasticity is favorable if {112}<111> twin system has a high Schmid factor (Yasuda and Umakoshi, 2011).

The Fe_3Ga single crystals with the stable and metastable $D0_3$ phase exhibit pseudoelasticity at a wide range of gallium concentration and temperature range (Umakoshi et al., 2007; Yasuda et al., 2007b, 2009, 2005, 2010; Yasuda and Umakoshi, 2011). The metastable $D0_3$ phase exists at a gallium concentration of approximately 23 at.% and temperatures below 650 °C (Ikeda et al., 2002). At room temperature and below, the twinning and detwinning of {112} pseudotwins primarily govern the transition from twinned to detwinned states, and hence no martensites are observed. This is because, similar to the bcc metals, a decrease in temperature suppresses the nucleation of a {110}<111> slip governing APB (antiphase boundary) formation without affecting the stress required to nucleate a {112}<111> twin. Therefore for a given stress at low temperature, it is much easier to nucleate a twin than a slip dislocation. The forthcoming analysis in the present paper focuses on pseudotwinning, albeit various mechanisms contribute to pseudoelasticity. Therefore our theoretical analysis is relevant to the experimentally observed pseudotwins in Fe_3GaB crystals annealed in the $D0_3$ phase and deformed at low temperatures.

The present work is based on a simultaneous "bottom-up" approach ranging from atomistic to macroscale to analyze the potential twinning in Fe_3GaB (see Fig. 2). On an atomic scale, we establish the energy barriers associated with the twinning process noting the transition of interstitial sites during shearing. The energy barriers are then employed into the atomistic–micromechanical approach, utilizing Peierls Nabarro formalism and Eshelbian anisotropic elasticity at micro-scale. During the course, we investigate solute distribution around the twinning dislocation and the interaction energies associated with the boron in the octahedral position. We finally develop a macroscale twinning stress model for Fe_3GaB.

2. Atomistic simulations

The first-principles Density Functional Theory (DFT) calculations were carried out to calculate the systems total-energy. We utilized the Vienna ab initio Simulations Package (VASP) with the projector augmented wave (PAW) method and the generalized gradient approximation (GGA) as implementations of DFT (Kresse and Furthmuller, 1996; Kresse and Hafner, 1993). In our calculations, we used a $9 \times 9 \times 9$ Monkhorst Pack *k*-point meshes for the Brillouion-zone integration to ensure the convergence of results. Ionic relaxation was performed by a conjugate gradient algorithm and stopped when absolute values of internal forces were smaller than 5×10^{-3} eV/A°. The energy cut-off of 350 eV was used for the plane-wave basis set. The total energy was converged to less than 10^{-5} eV per atom. For Generalized Planar Fault Energy (GPFE)

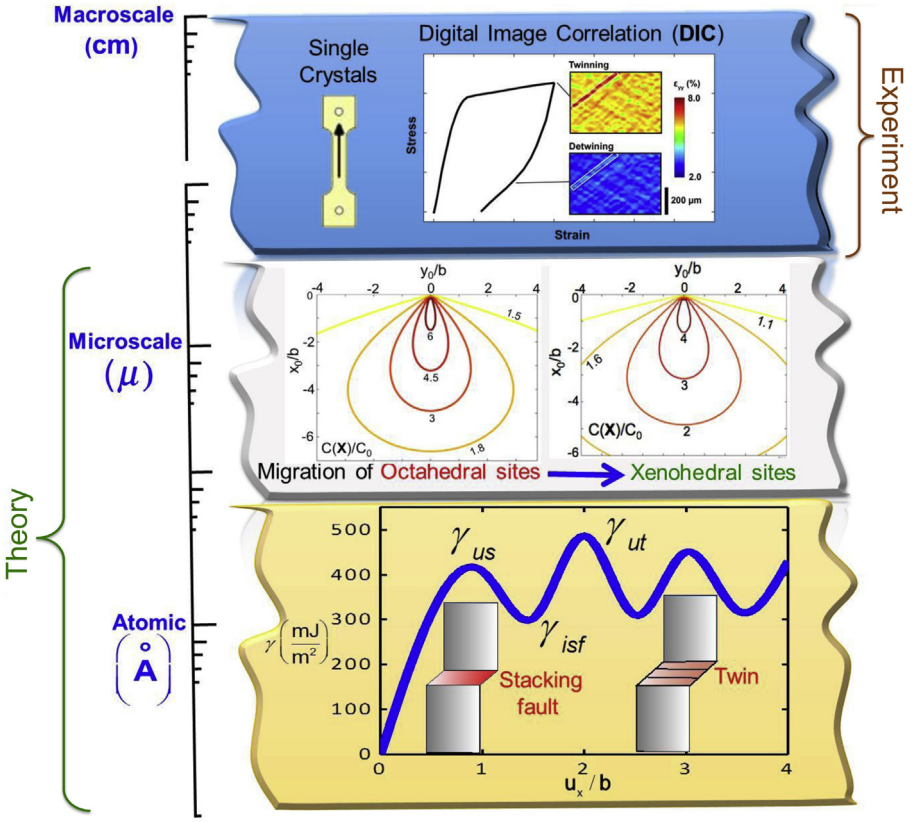

Fig. 2. Multiple length scales associated with the present analysis.

calculations, atoms relaxations including perpendicular directions to the fault plane, was allowed for minimizing the short-range interaction between misfitted layers near to the fault plane. During the relaxation process, atoms avoided coming too close to each other, and the total energy of the deformed crystal was minimized.

2.1. $D0_3$ structure and Generalized Planar Fault Energy (GPFE)

Fig. 3 illustrates the $D0_3$ structure of Fe_3Ga, and the positions of Fe and Ga are clearly shown. The unit cell of $D0_3$ consists of eight cubic sublattices. Four sublattices are B2 like structures while the remaining are of pure bcc types. All eight nearest neighbors of the first type of Fe sites are Fe atoms, whereas the second Fe sites are surrounded by four Fe and four Ga nearest neighbors. Fig. 3 also shows the {112}<111> twinning system. The boron solutes, when added to the pure crystal, can occupy the octahedral or tetrahedral sites depending on the minimum structural energy, and modify the lattice parameters. We calculated the lattice parameters for pure Fe_3Ga, and Fe_3GaB occupying both the octahedral and tetrahedral positions and are shown in Table 1. However, in actual crystals, the preference of one site over the other depends on the minimum energy of the Fe_3GaB system.

Fig. 4(a and b) show the octahedral and tetrahedral positions projected on a {100} plane for a cubic system. However, in real crystals boron atoms are observed to occupy the octahedral positions because of the lower structural energy compared to the tetrahedral site. We find that in the case of tetrahedral interstice, the minimum structural energy is −7.094 eV/atom while for the octahedral position, the minimum energy is found to be −7.14 eV/atom. We also observe that the addition of boron reduces the energy of the pure crystal by almost 50 meV/atom.

Fig. 5 shows the pseudotwin in $D0_3$ Fe_3Ga. It occurs by the subsequent motion of a/12<111> twinning partials on consecutive {112} planes where 'a = $2a_0$' is the lattice parameter. As opposed to a reflective twin, the atomic structure formed by shearing consecutive {112} planes do not form a mirror symmetry.

As seen in Fig. 5, different species of atoms occupy mirror plane *E*, and hence the term 'pseudotwin' is used. Fig. 6 shows the GPFE (Kibey et al., 2007; Ojha et al., 2014; Vitek, 1968) for Fe_3GaB required to create a three layer pseudotwin. The term γ_{us} represents the energy barrier required to form a first layer fault, γ_{isf} represents the first layer intrinsic stacking fault energy, γ_{ut} represents the additional energy barrier required to form a second layer fault, $2\gamma_{tsf}$ represents the stable second layer fault energy, and γ_{tbm} represents the twin boundary migration energy which is the difference between γ_{ut} and $2\gamma_{tsf}$. Unlike NiTi where fault energy increases with increase in twin layers, the GPFE curve is stabilized in Fe_3Ga and Fe_3GaB suggesting that twin formation and migration is energetically favorable (Ezaz et al., 2011). We obtained the GPFE curves for both cases where boron occupies the tetrahedral and octahedral positions (Fig. 6). Nonetheless, we will limit our analysis to octahedral interstitial to be consistent with the earlier experimental works (Gao et al., 2009), and the energy results reported in Table 1. It should be noted that the boron solutes for the case of octahedral sites are pushed further into the improper sites which lie along the close packed directions (hereafter, we refer these improper sites as the "xenohedral" sites, and will be discussed later). Therefore, γ_{us} in Fig. 6 for the octahedral case represents the energy barrier to nucleate a first layer fault ($u_x/b = 1.5$) when the solute is in the octahedral position. Subsequent shearing for $u_x/b > 1.5$, the GPFE represents the energy barrier to overcome the energy where boron occupies the xenohedral sites.

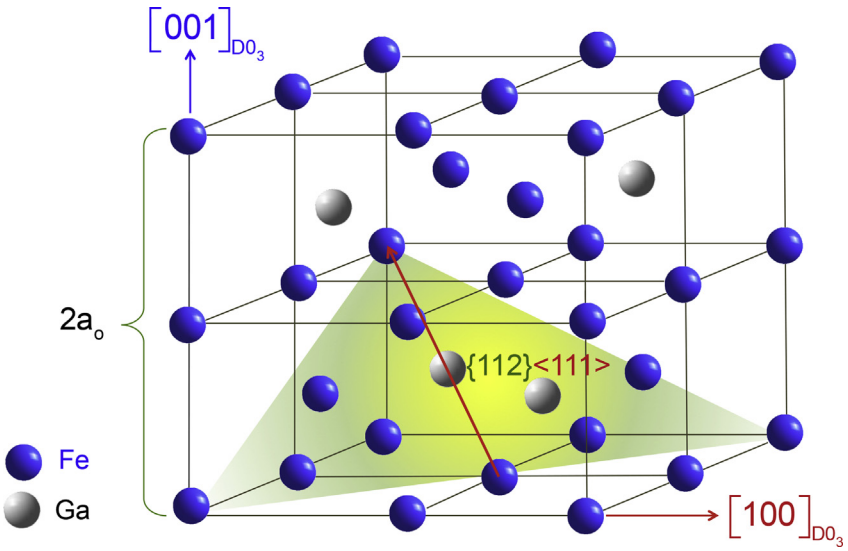

Fig. 3. $D0_3$ structure of Fe_3Ga. The shaded plane is the {112}<111> twinning plane.

Table 1
Lattice parameters and the structural energies of Fe_3Ga and Fe_3GaB occupying the octahedral and tetrahedral sites.

Structure of Fe_3Ga	Lattice type	Structural energy (eV/atom)	Lattice parameter (A^o)	
			This study	Experiments[a]
Pure Fe_3Ga	bcc	−7.09	5.828	5.8295
Fe_3Ga–B (Octahedral)	bcc	−7.14	5.833	–
Fe_3Ga–B (Tetrahedral)	bcc	−7.094	5.841	–

[a] Data taken from Ref. (Srisukhumbowornchai and Guruswamy, 2001, 2002).

3. Modeling of pseudotwinning

It has now been well established that twin nucleation in metals are initiated by pre-existing dislocation configuration (Sleeswyk, 1963) or from a region of high stress concentration such as grain boundaries and inclusions (Marcinkowski and Sree Harsha, 1968). Fig. 7 shows the schematic of the twinning process where each of the twinning partials is associated with the solute atmosphere. With the growth of multiple layers, the twin assumes a semi-lenticular morphology, as validated by experimental observations (Jin and Bieler, 1995; Zhang, 1999). Once the first partial dislocation is nucleated, it creates an

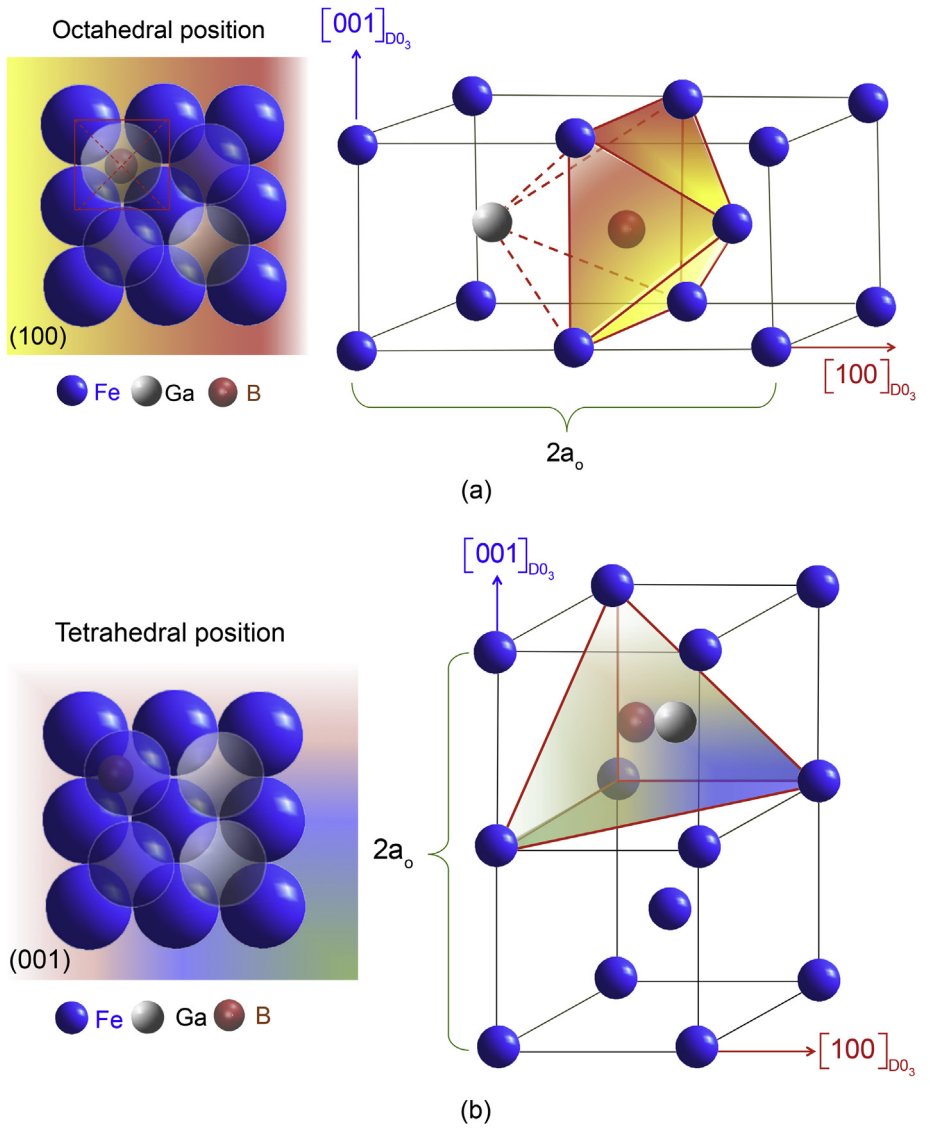

Fig. 4. (a) Interstitial boron occupying the octahedral site. Projection on {110} plane is shown. (b) Boron occupying the tetrahedral site. Note that only two cubic sublattices of DO_3 structure are shown for clarity.

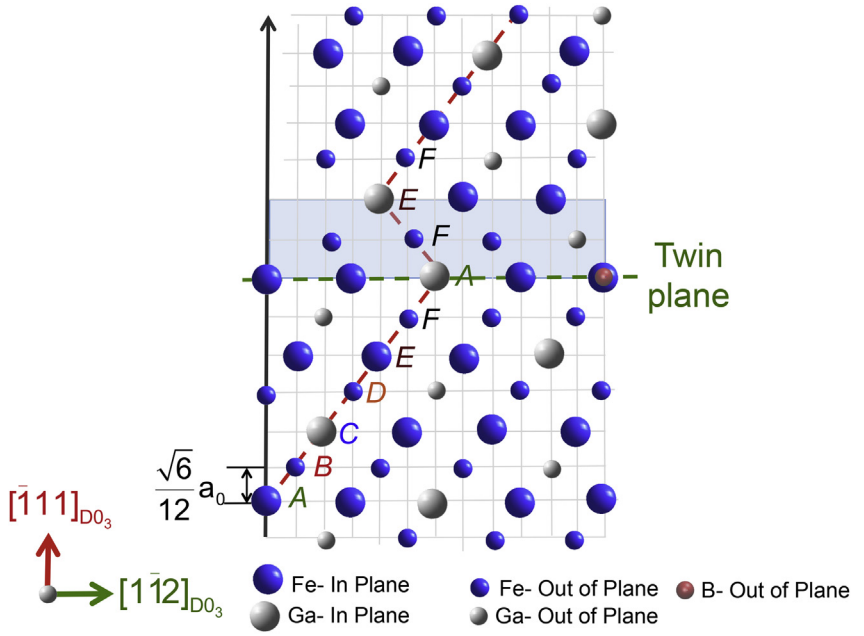

Fig. 5. Three layer {112}<111> pseudotwin in Fe_3GaB. Pseudotwins can be created by the passage of a/12<111> partial dislocations on consecutive {112} planes.

intrinsic stacking fault energy, and subsequent trailing dislocations nucleate forming a multilayer twin. While the twinning stress expressions proposed earlier account for elastic interactions of dislocations in isotropic medium (Lagerlof, 1994; Sleeswyk, 1963), we undertake anisotropic calculations in the present work. Consider a twin with the dislocations arrangement shown in Fig. 7. We write the total energy (E_{total}) of the dislocation configuration as follows:

$$E_{total} = E_{D-I} + E_{D-D} + E_D + E_I + E_{GPFE} - W \tag{2}$$

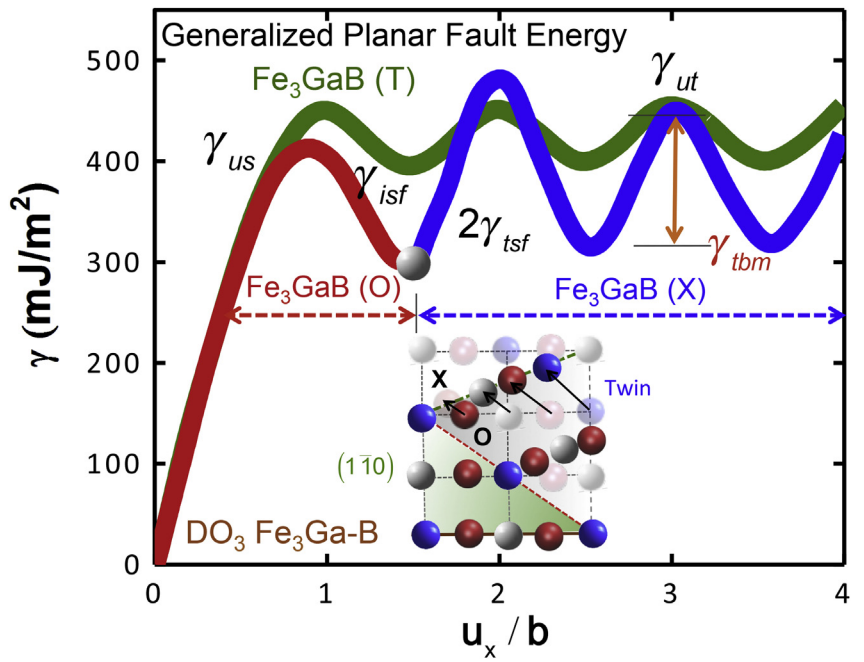

Fig. 6. Generalized Planar Fault Energy (GPFE) for F_3Ga-B occupying octahedral and tetrahedral sites. The letters T, O and X represent tetrahedral, octahedral and xenohedral sites respectively

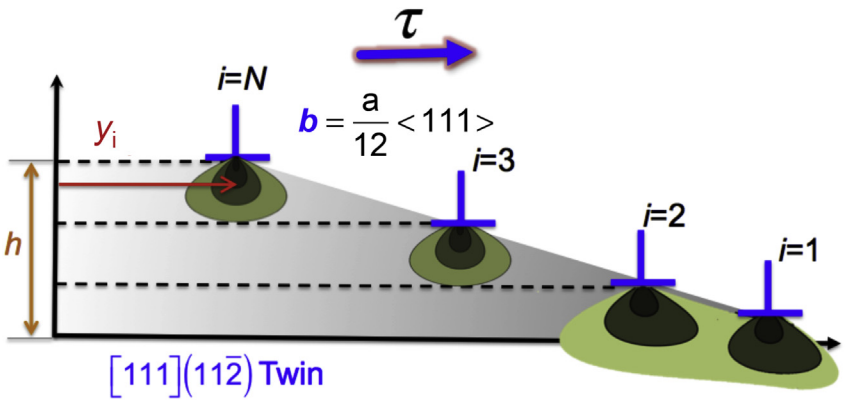

Fig. 7. Schematic of twin nucleation in bcc crystal on {112} plane.

where E_{D-I} is the dislocation–interstitial interaction energy, E_{D-D} is the dislocation–dislocation interaction energy, E_D is the self energy of the dislocation, E_I is the strain energy of the interstitial, E_{GPFE} is the misfit energy which represents the periodic energy barrier required to move the dislocation in an elastic crystal, and W is the applied work. We describe each of the parameters in detail in the following sections.

3.1. Concentration dependence

It is well known that the strain energy of the crystal is reduced when the dislocations are surrounded by solutes (Graham and Sines, 1966). The cluster of atoms commonly referred to as 'Cottrell atmosphere' tend to lock the dislocations and a relatively high stress is required to move the dislocations depending on the interaction energy between the dislocation and the solute. This generally contributes to strengthening in metals (Fleischer, 1962b, 1963; Graham and Sines, 1966). The concentration of the solutes around the dislocation can be approximated using a Fermi–Dirac equation given by (Beshers, 1958):

$$C(X) = \frac{C_0}{\frac{C_0}{\beta N_L} + \left(1 - \frac{C_0}{\beta N_L}\right)\exp\left(\frac{E_{\text{int}}}{kT}\right)} \tag{3}$$

Where C_0 is the remote concentration of solute atoms expressed as atoms per unit volume, β is the ratio of available solute sites to solvent atoms, N_L is the number of solute atoms per unit cell volume, and $C(X)$ is the concentration of solute atoms as a function of X. T and k are the absolute temperature and Boltzmann constant, respectively. In case of bcc, there are 18 octahedral and 24 tetrahedral sites. It is seen from equation (3) that $C(X)$ depends on the interaction energy term E_{int} between dislocation and solute. The interaction energy term and the solute concentration profile results are discussed next.

3.2. Interaction energy between dislocations and solutes, $E_{D\text{-}I}$

Consider boron atoms in the $D0_3$ lattice of Fe_3Ga. In order to estimate the interaction energy between dislocations and the solute, we need to know the stress field of a dislocation that interacts with the strain field of the solute. Eshelby et al. (1953) introduced the method for obtaining the stress field of a dislocation in an anisotropic crystal, however closed form solutions are possible only when the dislocation line lies along certain symmetry directions such as <100> and <110> directions of the cubic crystal. Anisotropic calculations have been done earlier to find the elastic interaction energy between the dislocations and the tetragonal defects in cubic medium (Graham and Sines, 1966). We note that in the present analysis, this is not the case because the screw dislocation lies along the <111> direction. We use the method developed earlier (Head, 1964a,b) to solve for the stress dislocations lying along <111> direction of the cubic lattice, and find the interaction energy of the dislocation and the solute as follows:

$$E_{\text{int}} = -\oint_V \sigma_{pq}^{disl}\varepsilon_{pq}^{solute}dV \tag{4}$$

where σ_{pq}^{disl} is the stress field of a dislocation in cubic medium and $\varepsilon_{pq}^{solute}$ is the tetragonal strain field of the solute.

Consider that a screw dislocation lies along the <111> direction as shown in Fig. 8 (Cochardt et al., 1955). At a distance $|\vec{r}|$ from the dislocation, there is a unit cell with axes 1, 2, 3 whose directions are [100], [010], [001] respectively. Consider another coordinate frame $x'y'z'$ where z' is parallel to the dislocation Burgers vector and y' is along the radius vector $\vec{r}$. The projection

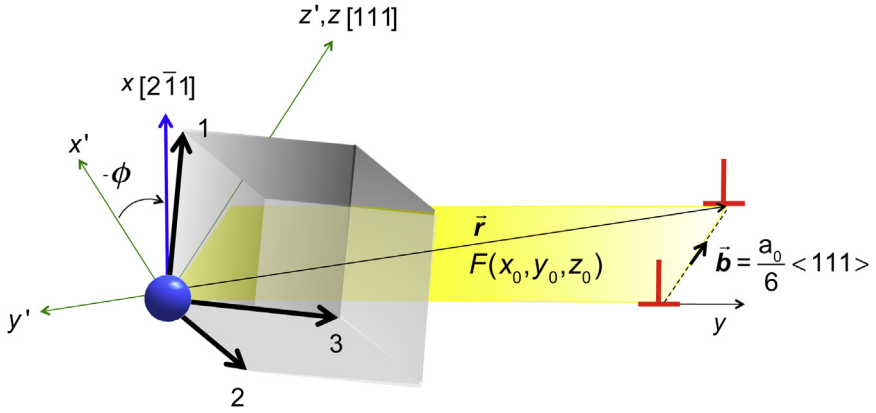

Fig. 8. Schematic showing the coordinate systems for screw dislocation, and its interaction with the solute.

of the 1-axis in the x'–y' plane is the $[2\bar{1}1]$ direction and the angle between the x' direction and the $[2\bar{1}1]$ direction is defined as ϕ. In the cubic coordinate frame, the strain tensor of the tetragonal distortion is given by:

$$\varepsilon = \begin{pmatrix} \varepsilon_{11} & 0 & 0 \\ 0 & \varepsilon_{22} & 0 \\ 0 & 0 & \varepsilon_{22} \end{pmatrix} = \begin{pmatrix} 0.43 & 0 & 0 \\ 0 & -0.04 & 0 \\ 0 & 0 & -0.04 \end{pmatrix} \tag{5}$$

The tetragonal strain in equation (5) is obtained for an octahedrally located boron solute using DFT simulations in conjunction with the visualization code developed by Li (2003). The exact expressions for the stress field σ_{pq}^{disl} of the dislocation lying along <111> direction in $x'y'z'$ coordinate frame can be written as follows (Cochardt et al., 1955):

$$\sigma' = \frac{C_{44} bH}{2\pi r} \begin{pmatrix} 0 & 0 & 1 \\ 0 & 0 & 0 \\ 1 & 0 & 0 \end{pmatrix} \tag{6}$$

In the above stress equation (6), H is the parameter that involves the orientation of the screw dislocation (Head, 1964a,b). The parameter H can be written as follows:

$$H \approx 1 - 4\left(1 - A^{-1/2}\right)\left(\alpha^2\beta^2 + \gamma^2\alpha^2 + \beta^2\gamma^2\right)$$

where A is the Zener's anisotropy ratio of the crystal equal to $2C_{44}/(C_{11}-C_{12})$ and α, β, γ are the orientation of the dislocation line with respect to the cubic axes. The terms C_{11}, C_{12} and C_{44} are the elastic constants of a cubic crystal in Voigt notation. It is important to note that in order to calculate the interaction energy, either stress or strain tensor should be transformed into the coordinates of the other. Transforming the strain tensor (5) into the stress coordinates, we have the following:

$$\varepsilon' = \varepsilon_{x'z'} = \frac{\sqrt{2}}{3}(\varepsilon_{11} - \varepsilon_{22})\cos\varphi \tag{7}$$

while other strain components do not contribute to the interaction energy. The strain terms ε_{11} and ε_{22} are given in equation (5). Fig. 9 shows an example of the concentration profile around a partial dislocation. In this case, the solutes are in the octahedral sites. We plot the normalized results where the contours 6, 4.5, 3, 1.8 and 1.5C(X)/C_0 are shown. It should be noted that higher solute concentration segregate below the dislocation thereby reducing the total strain energy, and making the dislocations difficult to move. Next, in order to compute the elevation in stress required for pseudotwinning, the stress field of a solute that must be overcome by a dislocation must be calculated. We are interested in determining the stress field due to the cluster of atoms at a spatial location, r from the dislocation. For this, we first obtain the stress field due to a single atom, and use the linear superposition to find the stresses due to the cluster of atoms $C(X)$ (Andrews et al., 2000). Mura and Cheng (1977) have provided the method of obtaining the stress field of a solute in an anisotropic medium in detail. Following their work, we have the following expression in spherical coordinates for the stress field (Mura and Cheng, 1977):

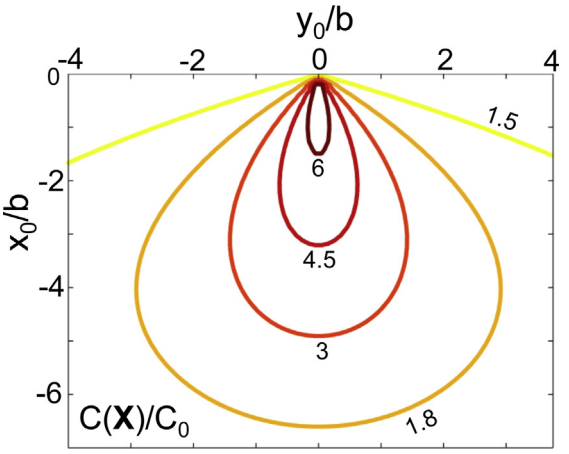

Fig. 9. Concentration of interstitial atoms, C(**X**)/C_0, around the partial dislocation.

$$\sigma_{pq} = C_{pqik}\left\{\begin{array}{l} \dfrac{\rho^3}{8\pi^2}\varepsilon^*_{mn}\displaystyle\int_{S^*} C_{jlmn}\bar{\xi}_l\bar{\xi}_k N_{ij}(\bar{\xi})D^{-1}(\bar{\xi})\varsigma^{-3}(\bar{\xi})dS(\bar{\xi}) \\ -\dfrac{\varepsilon^*_{mn}}{2\pi}\displaystyle\oint_L C_{jlmn}\bar{\xi}_l\bar{\xi}_k N_{ij}(\bar{\xi})D^{-1}(\bar{\xi})\left|r\right|^{-1}\left|r\right|^{-1}d\theta(\bar{\xi}) \end{array}\right\} \tag{8}$$

The term C_{pqik} (or C_{jlmn}) is the fourth order elastic modulus tensor for the cubic crystal, ρ is the radius of the solute, N_{ij} is the cofactor and D is the determinant of the 3×3 matrix with elements $C_{irjs}\bar{\xi}_r\bar{\xi}_s$. Here, $\bar{\xi}$ is a vector denoting the position of surface element dS from the center of the inclusion, and ε^*_{mn} is a constant misfit strain. The term $|r|$ is the magnitude of the vector $\vec{r}$ from the inclusion to the point outside the inclusion, and is written as follows:

$$|r| = \sqrt{r_i r_i}$$

The components of r are given as follows:

$$r_1 = x/\rho,\ \ r_2 = y/\rho,\ \ r_3 = z/\rho$$

Similarly, $\bar{\varsigma}$ is a vector, the components of which are given as follows:

$$\bar{\varsigma}_1 = \rho\bar{\xi}_1/\varsigma,\ \ \bar{\varsigma}_2 = \rho\bar{\xi}_2/\varsigma,\ \ \bar{\varsigma}_3 = \rho\bar{\xi}_3/\varsigma$$

$$\varsigma^2 = (\rho\bar{\xi}_1)^2 + (\rho\bar{\xi}_2)^2 + (\rho\bar{\xi}_3)^2$$

S^* is the subdomain on S^2 satisfying the following condition-

$$\bar{\varsigma}\cdot r \le 1$$

and the integral along L is performed along the circle on S^2 given by

$$\bar{\varsigma}\cdot r = 1$$

The numerical solution scheme for solving equation (8) is provided in detail in Mura and Cheng (1977) and Mori et al. (1978). The reader is advised to see Fig. 4 in Mura and Cheng (1977) for the schematic description of terms.

It is important to note that equation (8) gives the elastic stress field outside a single inclusion. For a remote solute concentration of $C(X)$, we use the linear superposition principle to find the stress field generated by the cluster of solutes as follows (Andrews et al., 2000):

$$\sigma_{pq}^{total} = -\oint_V C(X)\sigma_{pq}(r,\theta,\Delta z')dV \tag{9}$$

The integral limits in equation (9) are based on a cylindrical space with inner radius as the radius (ρ) of the boron solute, and the outer radius as 500 ρ, an arbitrary cutoff radius where the contribution due to solute atoms is considered to be negligible. Although we are interested in determining the twinning stress in the presence of boron solutes, it is worthwhile investigating the force exerted by solutes on the dislocation. As an example, we show the force variation on the dislocation, F_1 in y direction, which is given by,

$$F_1 = b\int_{-\infty}^{+\infty} \sigma_{pq}^{total}(x,y,z)dy \tag{10}$$

Note that equation (10) depends on the solute concentration through the term σ_{pq}^{total}(see equation (9)). The normalized force variation ($F_i/(b\rho C_{44}\varepsilon^*)$) obtained upon solving equation (10) for the case of a single solute is shown in Fig. 10. We can vary $C(X)$ in equation (9), and evaluate the normalized force variations for different remote solute concentration. Finally, with σ_{pq}^{total} known from equation (9), the interaction energy between inclusions and the dislocation per unit length is given as follows (Mura, 1987):

$$E_{D-I} = -\oint_S \sigma_{pq}^{total}(r,\theta,\Delta z')\varepsilon dS \tag{11}$$

The integration is carried out over the domain S occupied by the inclusions.

3.3. Twinning dislocation interaction energy, $E_{D\text{-}D}$

The dislocations interaction energy in an anisotropic medium is given by (Head, 1964a,b),

$$E_{D-D} = \frac{Kb^2}{4\pi}\sum_{m}^{N-1}\left(\sum_{i=1}^{m}\ln\frac{L}{d_i} + \sum_{i=2}^{m}\ln\frac{L}{d_i} + \ldots.. + \sum_{i=N-1}^{m}\ln\frac{L}{d_i}\right) \quad \text{for } i = 1,2....N-1 \tag{12}$$

where d_i is the separation distance of the dislocations, L is the equilibrium separation distance under zero external stress, and K is defined as:

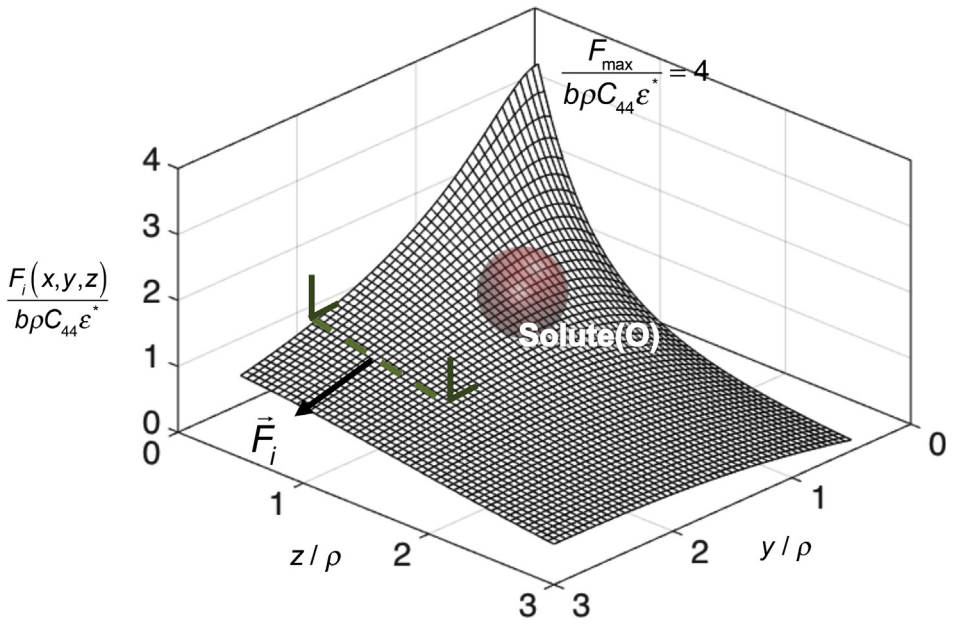

Fig. 10. Normalized force variation on the dislocation due to a single solute as a function of the dislocation position.

$$K = (C_{11} + C_{12})\left\{\frac{C_{44}(C_{11} - C_{12})}{C_{11}(C_{11} + C_{12} + 2C_{44})}\right\} \tag{13}$$

3.4. Twin boundary energy, E_{GPFE}

The disregistry function accounting for the interaction of multiple dislocations in y direction can be described by the following expression (Carrez et al., 2009; Joós et al., 1994).

$$f(y) = \frac{b}{2} + \frac{b}{\pi}\left(\tan^{-1}\left(\frac{y}{\zeta}\right) + \tan^{-1}\left(\frac{y - d_1}{\zeta}\right) + \ldots\ldots + \tan^{-1}\left(\frac{y - d_1 - d_2 - \ldots d_i}{\zeta}\right)\right) \quad \text{for } i = 1, 2, \ldots N-1 \tag{14}$$

where ζ represents the half-core width of the dislocation. The disregistry function $f(y)$ represents the relative displacement of the two half crystals in the twin plane along the y-direction.

Since slip and twinning are governed by different parts of the GPFE curve, the energy required to nucleate a slip and twin can be written respectively as

$$\gamma_{sf}(f(y)) = \gamma_{isf} + \left(\frac{\gamma_{us} - \gamma_{isf}}{2}\right)\left(1 - \cos\left(2\pi\frac{f(y)}{b}\right)\right) \quad \text{for } 0 \le f(y) \le b$$

$$\gamma_{twin}(f(y)) = \left(\frac{2\gamma_{tsf} + \gamma_{sf}}{2}\right) + \frac{1}{2}\left(\gamma_{ut} - \left(\frac{2\gamma_{tsf} + \gamma_{isf}}{2}\right)\right)\left(1 - \cos\left(2\pi\frac{f(y)}{b}\right)\right) \quad \text{for } 0 \le f(y) \le Nb$$

The twin boundary energy, E_{GPFE} based on the Peierls Nabarro formulation can be written as (Carrez et al., 2009; Joós et al., 1994)-

$$E_{GPFE}(d) = \sum_{m=-\infty}^{m=+\infty} \gamma_{SF}\{f(mb)\}b + (N-1)\sum_{m=-\infty}^{m=+\infty} \gamma_{twin}\{f(mb)\}b \tag{15}$$

3.5. Self-energy of dislocation line E_D, and the interstitial strain energy, E_I

The self energy of dislocation line in cubic medium is given by (Head, 1964a,b),

$$E_D = \frac{NKb^2}{4\pi}\ln\frac{R}{r_o} \tag{16}$$

where N is the total number of twinning partials, the parameter K is defined by expression (13), R is the radius of the dislocation strain field, and r_o is an effective core radius. Similarly, the total strain energy of the interstitial solute embedded in the matrix is given as follows (Eshelby, 1957):

$$E_I = -\frac{1}{2}\int_v \sigma_{ij}\epsilon^*_{ij}dV \tag{17}$$

where ϵ^*_{ij} is the misfit strain and σ_{ij} is the stress derived from ϵ^*_{ij} by Hooke's law. We note that the self-energy of the dislocation line, E_D, and the strain energy of the interstitial, E_I appear as constant terms in the total energy expression and hence, they do not contribute to the twinning stress.

3.6. Applied work, W

The work done in moving the dislocations is given by:

$$W = \sum_{i=1}^{N-1} \tau s h d_i \tag{18}$$

where τ is the applied stress, s is the twinning shear, and h is the height of the three layer twin nucleus.

Now, it is important to emphasize that the energy terms E_{D-I}, E_{D-D}, E_{GPFE} and W in equation (2) for E_{total} all have d_i dependence, where d_i is the separation distance between the dislocations. The term E_{D-I} in equation (11) incorporates d_i through the term r. We differentiate the total energy E_{total} with respect to d_i as follows:

$$\frac{\partial E_{total}}{\partial d_i} = 0 \quad \text{for } i = 1, 2, 3..... \tag{19}$$

For a given number of N dislocations forming the twin nucleus (equal to 3 in the present analysis), we have $(N-1)$ independent equations to solve for each d_i. Note that for three twinning dislocations, we solve for two separation distances d_1 and d_2. The critical twinning stress is then numerically obtained as the minimum applied stress that satisfies both the equations.

4. Experimental methods and results

Ingots of $FeGa_{24}B_1$ and $FeGa_{24}$ were sectioned into 4 mm × 4 mm × 10 mm compressive specimens. The specimens were homogenized at 1100 °C/48 h under vacuum, solution-treated at 800 °C/1 h and quenched in iced water, and successively annealed at 600 °C/10 h for $D0_3$ ordering. The specimen surfaces were polished using SiC paper and the grain boundaries were determined by the etchant containing 5 vol.% nitric acid and 95 vol.% methyl alcohol. The specimen surface for DIC strain measurements was successively polished with SiC paper up to P1500. The speckle pattern for DIC strain measurements was obtained using black paint and an Iwata Micron B airbrush. The images suited for DIC strain measurements were captured by means of a IMI model IMB-202 FT CCD camera (1600 × 1200 pixels) with a Navitar optical lens. Real time (*in-situ*) strain measurements were then obtained for a specimen region of approximately 3 mm × 4 mm with a resolution of 2.5 μm/px. One image (reference) was captured at zero load on the undeformed specimen, while during loading images were captured every two seconds. The correlation between the reference image and the deformed images was performed with commercial software (VIC-2D). The specimens were loaded under an MTS hydraulic load frame in displacement control under a constant strain rate of approximately 10^{-4} s^{-1}. An example of these experiments is shown in Fig. 11 for a $FeGa_{24}B_1$ specimen. Some of the analyzed grains in the DIC region show predominantly deformation by twinning, other by slip. We conducted detailed post-mortem analysis by polishing and etching the specimen in order to precisely detect the grains deformed by twinning (as show in the inset of Fig. 11) and the ones predominantly by slip. Further analyses were carried out using electron back-scattering diffraction in order to determine the grain orientation and to index the active twin systems via trace analysis.

The twin nucleation stress was then determined using the Schmid factor (0.49 in the present case) for the active twin system multiplied by the axial stress. In Fig. 11 we show an example of the local stress-strain curve calculated for a grain showing high density of twins. The axial strains reported in the curve were calculated averaging the axial strain contained in the selected grain. This enabled to precisely identify the twin nucleation stress. The stress-strain curve in Fig. 11 shows some pseudoelastic recovery upon unloading. The ratio of recoverability is generally lower than that of the single crystal specimen (see for example the curve shown in Fig. 1) as the grain boundaries curtail pseudoelasticity. The averaged critical twinning stresses for Fe_3Ga and Fe_3Ga-1 at.%B specimens are reported in Table 2.

5. Discussion of the results

Fig. 10 shows the normalized force exerted on one of the partial dislocations due to a single solute as a function of the distance from the solute obtained using equation (10). For solute concentration (C_0) of 0.5 at.%, 2 at.% and 4 at.%, the maximum

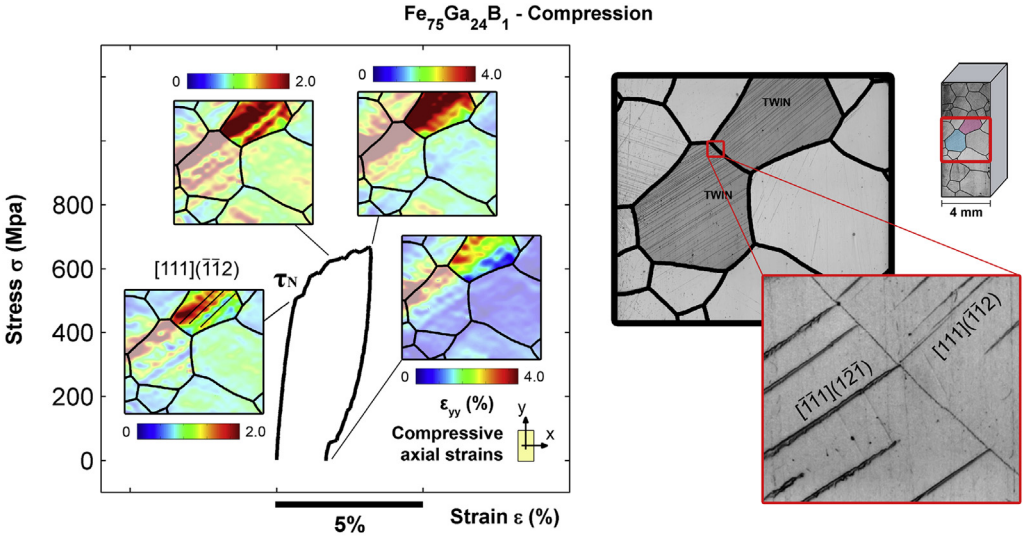

Fig. 11. The twinning-detwinning mechanism in Fe_3GaB during deformation captured with sub-grain strain measurements via digital image correlation. The critical twinning stress (τ^N) for Fe_3Ga-1 at.%B was obtained as 220 MPa (average of three tests).

values of the total normalized force were obtained as 6.17, 7.34 and 7.83 respectively (figures not shown in the paper). The elastic constants used in the present calculations for Fe_3Ga are $C_{11} = 181$ GPa, $C_{12} = 166$ GPa and $C_{44} = 126$ GPa (Zhang et al., 2010). Similarly, the {112}<111> shear moduli for Fe_3Ga with 0.5, 1, 2 and 4 at.% boron were obtained as 19, 22, 23 and 27 GPa respectively using methodology described by Wang and Sehitoglu (2014a). It is evident from Fig. 10 that the force exerted on the dislocation increases sharply at short distances from the solute reaching a maximum value of approximately 4 at the solute interface $(y/\rho, z/\rho)$ of (0.5,0.5), and falls off at larger distances. Based on the present analysis, in Table 2, we compare the critical twinning stresses for the Fe_3Ga with the Fe_3GaB system for different boron concentrations obtained using equation (19). The ideal twinning stress (Ogata et al., 2005) in Table 2 is calculated using equation, $\tau^{ideal}_{critical} = \pi\gamma_{tbm}/b$, where γ_{tbm} is the twin boundary migration energy reported in Table 3, and b is the Burgers vector of the twinning partial. The twinning stress of 235 MPa calculated using the present analysis for pure Fe_3Ga is consistent with the experimental twinning stress of 225–249 MPa (Yasuda et al., 2009) for the case of single crystal, and is much lower than the ideal twinning stress of 1860 MPa. Using present analysis, when pure Fe_3Ga is alloyed with 0.5 at.% boron at first, the increase in stress is maximum (38 MPa) while with further alloying (>0.5 at.%), the stress increment is less pronounced. Furthermore, the twinning stresses measured on the Fe_3Ga and Fe_3Ga-1 at.%B polycrystals using DIC strain measurements show that boron increases the twinning stress (see Table 2). Despite the experiments are made on polycrystal specimens (with a large grain size approximately >1 mm) and the influence of the grain boundaries cannot be neglected, the measured stresses provide a useful comparison between the Fe_3Ga and Fe_3GaB alloys, thus highlighting the effect of boron on the twinning stress elevation. The stress required to nucleate twins in Fe_3Ga was measured as 150 MPa, while for Fe_3Ga-1 at.% B as 220 MPa. These results confirm the trend captured with the present model. The reason behind the increase in twinning stress with an increase in boron content is the following. The number of boron solutes that can diffuse into the dislocation is limited because the addition of more boron solutes is no longer able to reduce the strain energy of the crystal (Cochardt et al., 1955). Therefore, an increase in solute concentration beyond a certain limit will no longer contribute to the increase in stress. Therefore, we note that the increase in solute concentration in stress elevation is more pronounced up to approximately 0.5 at.% beyond which we expect the stress values to saturate rapidly.

The reason behind this can be rationalized from energetic perspectives as well. We obtained the GPFE parameters for different concentrations of boron solutes, and are shown in Table 3. It is interesting to note that when 0.5 at.% boron is added to pure Fe_3Ga, the γ_{tbm} increases approximately by a factor of two, but with the higher concentration beyond 1 at.%, γ_{tbm} increases moderately. With an increase in γ_{tbm}, the twinning stress is expected to increase as well (Ojha et al., 2014). While further increase in boron concentration does not appreciably affect the γ_{tbm} values, the effect of boron on twinning stress level is not so significant beyond 1 at.%.

We note from Fig. 9 that the partial dislocation is surrounded by an atmosphere of boron solutes, and hence an additional stress is required to move the dislocations out of this atmosphere. Strengthening of metal matrix by tetragonal distortions has been well documented in the literature (Fleischer, 1962a,b; Graham and Sines, 1966), for example, the strengthening of Fe matrix by interstitial carbon atoms located octahedrally in the matrix. In case of deformation twinning in bcc iron in the presence of carbon solutes, it was observed that the stress necessary for twinning increased significantly from 333 MPa at 0.019 at.%C to 459 MPa at 0.089 at.%C (Magee et al., 1971). The increase in twinning stress arises from the fact that during the twin formation process, majority of the solutes in octahedral sites are sheared into the improper sites thereby increasing the stress for further deformation. It was also reported that with an increase in carbon concentration, the deformation mode changed from twinning to slip. In the present case, we observe that the increase in twinning stress is due to the increased interaction energy between the dislocations and the boron-induced tetragonal distortions which are asymmetrical unlike the uniform distortions created by the substitutional solutes. The phenomenological relationships (Fleischer, 1962a,b, 1963) considering the strengthening of metals by substitutional impurities show concentration dependence for the case of tetragonal distortion, and this has been successfully captured in the present analysis.

An analysis of the GPFE curves in Fig. 6 and their corresponding values reported in Table 3 reveals that with the boron in the tetrahedral site, the twin boundary migration energy is lower compared to the octahedral site. It is possible that if the boron solutes were to occupy the tetrahedral positions during shearing, the twin growth would be much easier contributing to enhanced ductility. Magee et al. (1971) have considered the effect of octahedral interstitials in the twinning of bcc metals. In fact, when a bcc crystal containing octahedral interstitials is sheared to form a twin, two-thirds of the solute atoms initially

Table 2
Comparison of twinning stress for pure Fe_3Ga and Fe_3GaB using our analysis with the ideal and experimental twinning stress values.

Material	Critical twinning stress (MPa)			
	Ideal	Present theory	Experiment[b] (Single crystal)	Experiment[a] (Polycrystal, this study)
Fe_3Ga	1860	235	225–249	150
Fe_3Ga-0.5 at.%B	3515	273	–	–
Fe_3Ga-1 at.%B	6582	290	–	220
Fe_3Ga-2 at.%B	7106	311	–	–
Fe_3Ga-4 at.%B	7405	326	–	–

[a] The critical twinning stress values for polycrystalline samples are based on sub-grain strain measurements with known orientation from EBSD analysis. The value is an average of 4 tests for Fe_3Ga and 3 tests for Fe_3Ga-1 at.%B.
[b] Data taken from Ref. (Yasuda et al., 2009, 2010).

Table 3
Predicted fault energies of a twin boundary for Fe_3Ga for different boron concentration. The units of fault energies are in mJ-m^{-2}.

Metals	γ_{us}^{twin}	γ_{isf}	γ_{ut}	$2\gamma_{tsf}$	γ_{tbm}
Fe_3Ga	170	150	200	150	50
Fe_3Ga-0.5 at.%B (Oct)	360	300	395	301	94
Fe_3Ga-1 at.%B (Oct)	407	303	486	310	176
Fe_3Ga-1 at.%B (Tet)	457	400	460	395	65
Fe_3Ga-2 at.%B (Oct)	457	367	560	370	190
Fe_3Ga-4 at.%B (Oct)	476	390	585	387	198

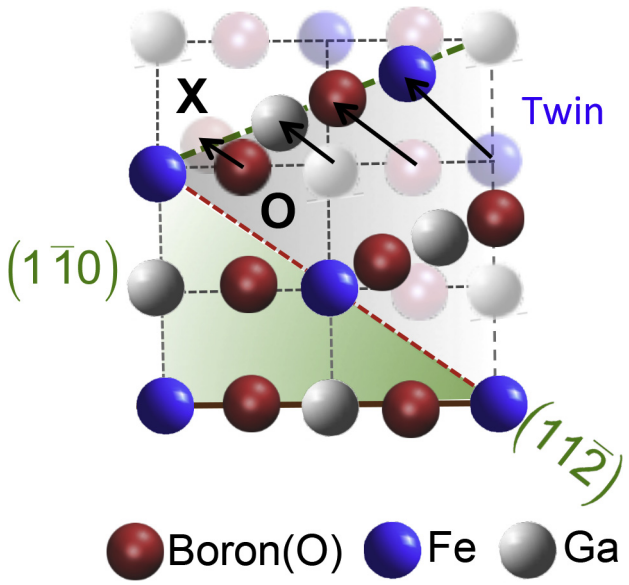

Fig. 12. The migration of an octahedral interstitial (O) to a xenohedral site (X) in a cubic lattice during twinning.

occupying the octahedral positions are sheared into the new sites which lie along the closed packed directions, for example the xenohedral sites, in the lattice of the twin as shown in Fig. 12. It is clear from Fig. 6 that γ_{tbm} for xenohedral interstice is much higher than that of the tetrahedral site. This potentially contributes an increased strength of Fe_3GaB crystal compared to pure Fe_3Ga by increasing the Peierls Nabarro barrier.

It should be noted that several assumptions are made during the course of the evaluation of the twinning stress. We neglect any thermal activation of the solute atoms, and the position of the boron solute atmosphere does not change during the dislocation motion.

6. Conclusion

Using anisotropic elasticity calculations, we established the twinning stress for Fe_3Ga alloyed with various boron concentrations. The preference of boron over octahedral site to tetrahedral site was found by considering the total structural energy of Fe_3Ga. It was found that the stress level required for pseudotwinning increased with an increase in boron concentration, and this was validated both theoretically and experimentally. Remarkable elevation in twinning stress was observed when pure Fe_3Ga was alloyed with 0.5 at.% boron while further increase in boron concentration increased the twinning stress more moderately. The GPFE curves for Fe_3GaB were established, and we observed that the increased twinning stress with increase in boron concentration in Fe_3Ga was due to the increase in twin boundary migration energy. We showed that when concentration of boron atoms is 0.5 at.%, a higher stress is required to nucleate a twin compared to unalloyed Fe_3Ga. We compare the twinning stress results from our analysis to experimental values for the Fe_3Ga single crystals and obtain an excellent agreement. Furthermore, the predictions in the present analysis can all be obtained from DFT without requiring any empirical constants.

Acknowledgments

This work was supported by the National Science Foundation, NSF CMMI-1300284. This support is gratefully acknowledged.

References

Andrews, S.D., Sehitoglu, H., Karaman, I., 2000. Constriction energy in the presence of a solute field. J. Appl. Phys. 87, 2194–2203.
Beshers, D.N., 1958. On the distribution of impurity atoms in the stress field of a dislocation. Acta Metall. 6, 521–523.
Carrez, P., Ferré, D., Cordier, P., 2009. Peierls–Nabarro modelling of dislocations in MgO from ambient pressure to 100 GPa. Model. Simul. Mater. Sci. Eng. 17, 035010.
Cochardt, A.W., Schoek, G., Wiedersich, H., 1955. Interaction between dislocations and interstitial atoms in body-centered cubic metals. Acta Metall. 3, 533–537.
Eshelby, J.D., 1957. The determination of the elastic field of an ellipsoidal inclusion, and related problems. In: Proceedings of the Royal Society of London A: Mathematical, Physical and Engineering Sciences, vol. 241. The Royal Society, pp. 376–396 no. 1226.
Eshelby, J.D., Read, W.T., Shockley, W., 1953. Anisotropic elasticity with applications to dislocation theory. Acta Metall. 1, 251–259.
Ezaz, T., Sehitoglu, H., Maier, H.J., 2011. Energetics of twinning in martensitic NiTi. Acta Mater. 59, 5893–5904.
Fleischer, R.L., 1962a. Rapid solution hardening, dislocation mobility, and the flow stress of crystals. J. Appl. Phys. 33, 3504–3508.
Fleischer, R.L., 1962b. Solution hardening by tetragonal distortions: application to irradiation hardening in FCC crystals. Acta Metall. 10, 835–842.
Fleischer, R.L., 1963. Substitutional solution hardening. Acta Metall. 11, 203–209.
Gall, K., Sehitoglu, H., Anderson, R., Karaman, I., Chumlyakov, Y.I., Kireeva, I.V., 2001. On the mechanical behavior of single crystal NiTi shape memory alloys and related polycrystalline phenomenon, micromechanics and micromechanisms of deformation and fracture. In: Honor of Professor Ali S Argon, 1999, 1–2 ed. Elsevier, Switzerland, pp. 85–92.
Gao, X., Li, J., Zhu, J., Li, J., Zhang, M., 2009. Effect of B and Cr on mechanical properties and magnetostriction of iron-gallium alloy. Mater. Trans. 50, 1959–1963.
Graham, L.J., Sines, G., 1966. Elastic interaction between dislocations and tetragonal defects in anisotropic sodium chloride. J. Appl. Phys. 37, 4207–4215.
Hartl, D.J., Chatzigeorgiou, G., Lagoudas, D.C., 2010. Three-dimensional modeling and numerical analysis of rate-dependent irrecoverable deformation in shape memory alloys. Int. J. Plast. 26 (10), 1485–1507.
Head, A.K., 1964a. The [111] dislocation in a cubic crystal. phys. status solidi b 6, 461–465.
Head, A.K., 1964b. The energy of a screw dislocation in a cubic crystal. phys. status solidi b 5, 51–54.
Ikeda, O., Kainuma, R., Ohnuma, I., Fukamichi, K., Ishida, K., 2002. Phase equilibria and stability of ordered bcc phases in the Fe-rich portion of the Fe–Ga system. J. Alloy. Compd. 347, 198–205.
Jin, Z., Bieler, T.R., 1995. An in-situ observation of mechanical twin nucleation and propagation in TiAl. Philos. Mag. A 71, 925–947.
Joós, B., Ren, Q., Duesbery, M.S., 1994. Peierls-Nabarro model of dislocations in silicon with generalized stacking-fault restoring forces. Phys. Rev. B 50, 5890–5898.
Kibey, S., Liu, J.B., Johnson, D.D., Sehitoglu, H., 2007. Predicting twinning stress in fcc metals: linking twin-energy pathways to twin nucleation. Acta Mater. 55, 6843.
Kresse, G., Furthmuller, J., 1996. Efficient iterative schemes for ab initio total-energy calculations using a plane-wave basis set. Phys. Rev. B Condens. Matter 54, 11169.
Kresse, G., Hafner, J., 1993. Ab initio molecular dynamics for open-shell transition metals. Phys. Rev. B Condens. Matter 48, 13115.
Lagerlof, K.P.D., 1994. A Model Describing Deformation Twinning in BCC Metals, p. 601. Switzerland.
Li, J., 2003. AtomEye: an efficient atomistic configuration viewer. Model. Simul. Mater. Sci. Eng. 11, 173.
Magee, C.L., Hoffman, D.W., Davies, R.G., 1971. The effect of interstitial solutes on the twinning stress of bcc metals. Philos. Mag. 23, 1531–1540.
Marcinkowski, M., Sree Harsha, K., 1968. Numerical analysis of deformation twin behavior. Small static twin lamellas. J. Appl. Phys. 39, 6063–6070.
Mori, T., Cheng, P.C., Kato, M., Mura, T., 1978. Elastic strain energies of precipitates and periodically distributed inclusions in anisotropic media. Acta Metall. 26, 1435–1441.
Moumni, Z., Zaki, W., Nguyen, Q.S., 2008. Theoretical and numerical modeling of solid–solid phase change: application to the description of the thermomechanical behavior of shape memory alloys. Int. J. Plast. 24, 614–645.
Mura, T., 1987. Micromechanics of Defects in Solids. Springer Science & Business Media.
Mura, T., Cheng, P.C., 1977. The elastic field outside an ellipsoidal inclusion. J. Appl. Mech. 44, 591–594.
Ogata, S., Ju, L., Yip, S., 2005. Energy landscape of deformation twinning in bcc and fcc metals. Phys. Rev. B Condens. Matter Mater. Phys. 71, 224102.
Ojha, A., Sehitoglu, H., Patriarca, L., Maier, H.J., 2014. Twin nucleation in Fe-based bcc alloys—modeling and experiments. Model. Simul. Mater. Sci. Eng. 22, 075010.
Otsuka, K., Wayman, C.M., 1998. Shape Memory Materials. Cambridge University Press, Cambridge.
Sleeswyk, A.W., 1963. 111 screw dislocations and the nucleation of {112} 111 twins in the b.c.c. lattice. Philos. Mag. 8, 1467.
Srisukhumbowornchai, N., Guruswamy, S., 2001. Large magnetostriction in directionally solidified FeGa and FeGaAl alloys. J. Appl. Phys. 90, 5680–5688.
Srisukhumbowornchai, N., Guruswamy, S., 2002. Influence of ordering on the magnetostriction of Fe–27.5 at.% Ga alloys. J. Appl. Phys. 92, 5371–5379.
Tanaka, K., Kobayashi, S., Sato, Y., 1986. Thermomechanics of transformation pseudoelasticity and shape memory effect in alloys. Int. J. Plast. 2, 59–72.
Thamburaja, P., Anand, L., 2002. Superelastic behavior in tension–torsion of an initially-textured Ti–Ni shape-memory alloy. Int. J. Plast. 18, 1607–1617.
Umakoshi, Y., Nakajima, T., Yasuda, H.Y., 2007. Effects of dislocation and microstructure on pseudoelasticity in $D0_3$-Type Fe_3Al single crystals. In: Materials Research Society Symposium Proceedings. Cambridge Univ Press, p. 33.
Umakoshi, Y., Yasuda, H.Y., Nakajima, T., Nakano, K., Yamaoka, K., Ueda, M., 2005. Effect of Al concentration on pseudoelasticity in Fe_3Al single crystals. Acta Mater. 53, 5343–5351.
Vitek, V., 1968. Intrinsic stacking faults in body-centred cubic crystals. Philos. Mag. 18, 773.
Wang, J., Sehitoglu, H., 2014a. Martensite modulus dilemma in monoclinic NiTi-theory and experiments. Int. J. Plast. 61, 17–31.
Wang, J., Sehitoglu, H., 2014b. Modeling of pseudotwinning in Fe 3 Ga. Model. Simul. Mater. Sci. Eng. 22, 055008.
Wang, X.M., Xu, B.X., Yue, Z.F., 2008. Micromechanical modelling of the effect of plastic deformation on the mechanical behaviour in pseudoelastic shape memory alloys. Int. J. Plast. 24, 1307–1332.
Yasuda, H., Aoki, M., Takaoka, A., Umakoshi, Y., 2005. Pseudoelasticity in Fe_3Ga single crystals. Scr. Mater. 53, 253–257.
Yasuda, H., Nakajima, T., Umakoshi, Y., 2007a. Temperature dependence of pseudoelasticity in Fe_3Al single crystals. Intermetallics 15, 819–823.
Yasuda, H.Y., Aoki, M., Fukushima, K., Umakoshi, Y., 2007b. Pseudoelastic Behavior of Fe_3Ga Single Crystals with $D0_3$ Structure, 2006 MRS Fall Meeting, November 27, 2006–November 30, 2006. Materials Research Society, Boston, MA, United states, pp. 315–320.
Yasuda, H.Y., Aoki, M., Oda, Y., Fukushima, K., Umakoshi, Y., 2009. Unusual pseudoelastic behaviour of Fe_3Ga shape memory alloys. In: International Conference on Advanced Structural and Functional Materials Design 2008, 10–12 Nov. 2008. IOP Publishing Ltd, UK, p. 012053 (012056 pp.).
Yasuda, H.Y., Aoki, M., Umakoshi, Y., 2007c. Effect of the ordering process on pseudoelasticity in Fe_3Ga single crystals. Acta Mater. 55, 2407–2415.
Yasuda, H.Y., Kishimoto, T., Umakoshi, Y., 2010. Temperature dependence of twinning pseudoelasticity in Fe_3Ga single crystals. Mater. Trans. 51, 2196.
Yasuda, H.Y., Oda, Y., Kishimoto, T., Maruyama, T., 2013. Effect of Ga concentration on twinning pseudoelasticity in Fe–Ga single crystals. J. Alloy. Compd. 577, S563–S567.
Yasuda, H.Y., Umakoshi, Y., 2011. Pseudoelasticity of $D0_3$-type Fe_3Al and Fe_3Ga-based Alloys. Mater. Res. Soc. Symp. Proc. Cambridge Univ Press, p. 5.
Zhang, L., 1999. Twin-intersection-related nanotwinning in a heavily deformed gamma-TiAl-based alloy. Philos. Mag. Lett. 79, 49–54.
Zhang, Y.-N., Wu, R.-Q., Schurter, H.M., Flatau, A.B., 2010. Understanding of large auxetic properties of iron-gallium and iron-aluminum alloys. J. Appl. Phys. 108, 023513.